nature ecology & evolution

ARTICLES

PUBLISHED: 18 APRIL 2017 | VOLUME: 1 | ARTICLE NUMBER: 0132

Functional trait diversity maximizes ecosystem multifunctionality

Nicolas Gross[1,2,3†*], Yoann Le Bagousse-Pinguet[1†*], Pierre Liancourt[4†*], Miguel Berdugo[1], Nicholas J. Gotelli[5] and Fernando T. Maestre[1]

Understanding the relationship between biodiversity and ecosystem functioning has been a core ecological research topic over the past decades. Although a key hypothesis is that the diversity of functional traits determines ecosystem functioning, we do not know how much trait diversity is needed to maintain multiple ecosystem functions simultaneously (multifunctionality). Here, we uncovered a scaling relationship between the abundance distribution of two key plant functional traits (specific leaf area, maximum plant height) and multifunctionality in 124 dryland plant communities spread over all continents except Antarctica. For each trait, we found a strong empirical relationship between the skewness and the kurtosis of the trait distributions that cannot be explained by chance. This relationship predicted a strikingly high trait diversity within dryland plant communities, which was associated with a local maximization of multifunctionality. Skewness and kurtosis had a much stronger impact on multifunctionality than other important multifunctionality drivers such as species richness and aridity. The scaling relationship identified here quantifies how much trait diversity is required to maximize multifunctionality locally. Trait distributions can be used to predict the functional consequences of biodiversity loss in terrestrial ecosystems.

Global threats to biodiversity have motivated ecologists to better understand the relationship between biodiversity and ecosystem functioning[1] (BEF). Pioneering BEF experiments conducted in grasslands have shown a positive effect of species richness on ecosystem functioning[2,3], which has been later confirmed in many ecosystems[4–7]. However, there is a general consensus that it is not only the number of species *per se* that influences ecosystem functioning, but also the diversity and the abundance of their functional traits within communities[8–10]. As functional traits relate to how species acquire, share and conserve resources[11], they are often invoked to explain how species assemble within communities[12–14] and impact ecosystem functioning[8–10,15].

Higher trait diversity has been hypothesized to enhance ecosystem functioning because co-occurring species with contrasting trait values may exploit different resources, or the same resources on different spatial or temporal scales[2], and then may increase overall resource utilization[16]. This hypothesis has received support from BEF experiments[17] and empirical surveys[10,18,19]. However, most trait-based BEF studies have been conducted on local or regional scales[17,20], limiting our ability to generalize the effect of trait diversity on ecosystem functioning across ecosystems. Also, many studies have focused on single ecosystem functions (for example, productivity[10]), something that may provide a partial measure or even biased estimate of overall ecosystem functioning if trade-offs or synergies among functions are ignored[4,21,22]. Emerging empirical evidence suggests that higher trait diversity is especially important to sustain multiple ecosystem functions simultaneously[19,23] (multifunctionality). However, the extent to which trait diversity matters for multifunctionality remains unknown on a global scale.

Coupling a global survey of multifunctionality conducted in 124 perennial plant dryland communities from all continents except Antarctica[5] (Fig. 1) to an extensive trait database[24], we uncovered a scaling relationship between the abundance distribution of functional traits within communities and maximized multifunctionality. We quantified the 124 abundance distributions for specific leaf area (SLA) and maximum plant height (H; trait–abundance distributions)[25]. These two traits capture the global spectrum of plant form and function[26], and have been largely used to define species resource utilization strategies in terrestrial ecosystems[27]. Multifunctionality was quantified using five key ecosystem variables: plant productivity, soil enzymatic activities (phosphatase and β-glucosidase), ammonification and potential N transformation rate. These variables were uncorrelated (Supplementary Table 1) and are good proxies for nutrient cycling, biological productivity and soil fertility in global drylands[5,28] (see Methods for details).

We developed an analysis, inspired by multivariate optimization procedures that are used in various scientific fields (such as physics, geomorphology, climatology and particularly in economy, where it is employed for analysing budget portfolios maximizing benefits and minimizing costs in multiple investments[29]; see Supplementary Note 1 for more details), to link the trait–abundance distributions to multifunctionality. Specifically, our approach focused on the skewness and the kurtosis of the trait–abundance distributions[24,25,30–32]. Whereas the mean and the variance reflect the location and the scale of a distribution (that is, the dispersion of trait values within a community), the skewness and the kurtosis describe its shape. The skewness and the kurtosis complement the mean and the variance, particularly when assessing complex distributions that strongly deviate from the normal distribution[24,25,32] (Fig. 2).

[1]Departamento de Biología y Geología, Física y Química Inorgánica, Escuela Superior de Ciencias Experimentales y Tecnología, Universidad Rey Juan Carlos, C/ Tulipán s/n, 28933 Móstoles, Spain. [2]INRA, USC1339 Chizé (CEBC), F-79360 Villiers en Bois, France. [3]Centre d'étude biologique de Chizé, CNRS - Université La Rochelle (UMR 7372), F-79360 Villiers en Bois, France. [4]Institute of Botany, Czech Academy of Sciences, Dukelská 135, 379 82 Trebon, Czech Republic. [5]Department of Biology, University of Vermont, Burlington, Vermont 05405, USA. [†]These authors contributed equally to this work. *e-mail: gross@cebc.cnrs.fr; y.b-pinguet@orange.fr; pierre.liancourt@gmail.com

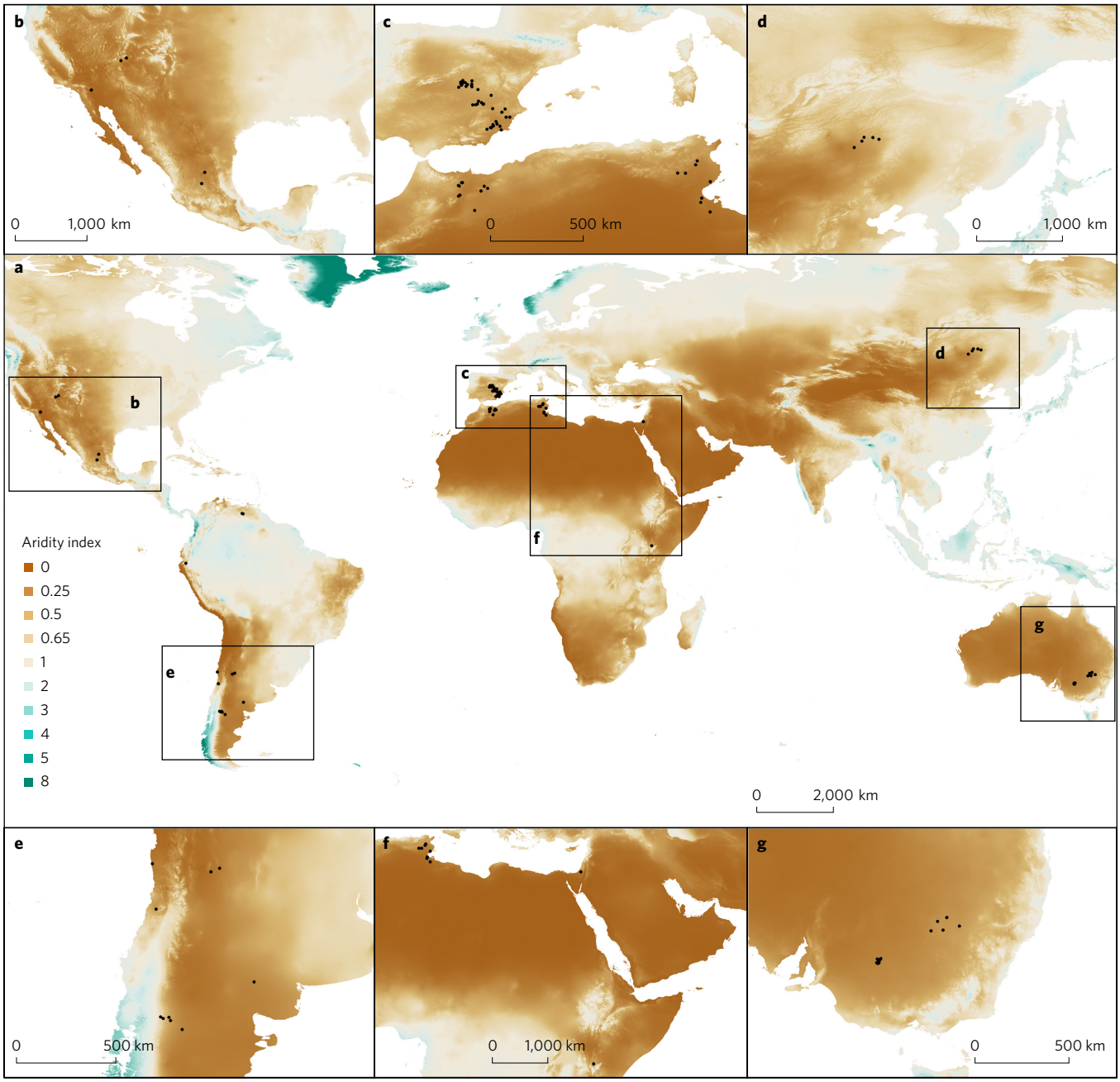

Figure 1 | Map of the 124 sampled drylands used in this study. a–g, Global map (**a**) and close-up maps of the sites located in North America (**b**), the Mediterranean Basin (**c**), China (**d**), South America (**e**), Africa and the Middle East (**f**) and Australia (**g**).

The skewness represents the asymmetry of the distributions. High negative or positive values of skewness occur when trait–abundance distributions are strongly left- or right-tailed, respectively, with a few abundant species that have extreme trait values compared with the bulk of the distribution. Skewed trait distributions typically result from phenomena such as asymmetric competition[33,34] or rapid environmental change[25,32]. Kurtosis represents the relative peakiness of the trait–abundance distribution and the heaviness of its tails, and is a measure of trait diversity[25,30,31]. High kurtosis values characterize peaked distributions, indicating a high abundance of species with similar trait values in a given community. High kurtosis values therefore reflect a low trait diversity[25], which might occur with strong environmental filtering[32]. Low kurtosis values reflect an even abundance distribution of trait values within the community, which implies the co-dominance of functionally contrasted species[32]. Low kurtosis reflects a high trait diversity[25], for example in the case of limiting similarity[35] or storage effects[36].

By analysing the shape of the 124 trait–abundance distributions, we first showed that trait diversity in dryland plant communities is generally higher than expected by chance. Then we showed that observed trait distributions in global drylands maximize multifunctionality, in agreement with the hypothesis that species with contrasting trait values collectively exploit a greater diversity of resources[2,16].

Results and discussion

The skewness–kurtosis relationship. Skewness (S) and kurtosis (K) are mathematically related according to the following skewness–kurtosis relationship[37] (SKR; Fig. 2):

$$K \geq \beta S^2 + \alpha \quad (1)$$

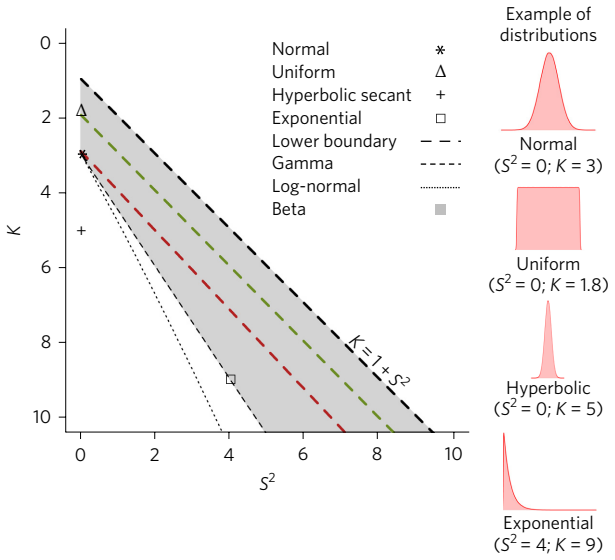

Figure 2 | SKR represented in the Cullen and Frey graph[37]. This graph represents the location of common distributions in the skewness–kurtosis space. The normal distribution represents a unique combination of skewness and kurtosis values of 0 and 3, respectively (see other example in the right panels). Families of trait distributions can be represented by a line for the gamma or log-normal distributions, and by a surface for the beta distribution. Note that the normal distribution represents a special case of the gamma and the log-normal distributions. The SKR has a lower boundary below which no kurtosis value can be observed for any degree of skewness. This lower boundary corresponds to the Bernoulli distribution. We also indicate the location of the empirical SKRs for SLA and *H* (green and red dashed lines, respectively; see main text). Low values of kurtosis indicate high trait diversity[25].

This inequality generates a mathematical constraint triangle on the possible values of skewness and kurtosis that can be observed for a community (Fig. 2; see also Supplementary Note 1 for detailed information). For a given set of distributions, an increase in S^2 will generate an increase in K, all other things being equal. In other words, as the trait–abundance distributions become more skewed, they also become more peaked, indicating a decrease in trait diversity[25]. The slope β of the SKR measures the strength of the relationship, that is, the extent to which trait diversity decreases as trait distributions become more skewed. The y-intercept α indicates the lowest kurtosis value at skewness = 0, which corresponds to the highest trait diversity predicted by a given SKR. Importantly, the inequality has a lower boundary that sets a limit to the minimal kurtosis value predicted for any degree of skewness, that is, the potential maximum trait diversity ($K = S^2 + 1$; Fig. 2). Although skewness and kurtosis separately provide valuable information on how trait diversity and abundance is distributed within communities, the SKR reveals the extent to which trait diversity is maximized.

Observed trait distributions in global drylands. The observed 124 trait–abundance distributions were highly heterogeneous and deviated from a symmetric normal distribution in most cases (Fig. 3). Consistent with equation (1), we observed a strong positive relationship between skewness and kurtosis of the distributions for both SLA and *H* (Fig. 3):

$$K_{SLA} \approx {S_{SLA}}^2 + 2 \quad (2)$$

$$K_H \approx {S_H}^2 + 3 \quad (3)$$

However, within the constraint triangle, there are a variety of possible SKRs that can be generated (Fig. 2). Empirical SKRs must then be compared with the null distribution of relationships that might arise by sampling random values within the constraint triangle. We used a Monte Carlo analysis to test whether the empirical SKRs differed from random expectations. These randomization tests used three null models that imposed increasing constraints on the species and trait pools.

In the first null model, we simulated the assembly of local plant communities from global pools of species and traits. In this null model, the local species number and trait values are randomly assigned to the null communities according to the hypothesis that the local environment may modify both local trait composition and species richness[38]. In the second null model, we fixed species richness at the site level, but allowed traits to vary across communities to decouple the effect of species richness and trait composition on local trait abundance distributions. In the third null model, we additionally constrained the range of trait values observed within community to be fixed. This third randomization procedure tested whether the distribution of trait values between co-occurring species maximized trait diversity locally (see Methods).

The empirical SKRs for SLA and *H* deviated strongly from the predictions of all three null models (Fig. 3). The slopes β and the y-intercepts α were all lower than expected by chance (Fig. 3 right panels; Table 1 left; see detailed results in Supplementary Note 2; Supplementary Fig. 2). Consequently, observed kurtosis values for each of the 124 trait–abundance distributions for both SLA and *H* were significantly closer than expected by chance to the lower boundary of the mathematical constraint triangle (Table 1 right; see the analysis on the distance to the lower boundary in Methods). In other words, observed kurtosis within communities was minimal after controlling for the degree of skewness in the data. Deviations from null expectations were consistent for all three null models (Table 1), so the results are robust to the details of how species and trait pools were constructed and randomized.

A general assembly rule in global drylands. Our findings have important implications for understanding community assembly in global drylands. The abundance and the diversity of trait values observed within the 124 communities evaluated cannot be observed by chance, and can be summarized by two empirical SKRs, one for *H* and another for SLA (Figs 2 and 3). Each of these SKRs defined a family of trait–abundance distributions in which the trait distribution of each studied community represents a particular instance of a more general distribution quantified on the biome scale (Fig. 2). These two biome-scale distributions predict that the kurtosis of trait distributions is always minimized (Fig. 3). Our study therefore uncovered a general 'assembly rule'[12,39]: across a variety of continents, species pools and environmental conditions, trait diversity is maximized within dryland plant communities.

For asymmetrical distributions ($S^2 > 0$; Fig. 2), lower kurtosis than expected by chance implies heavier-tailed distributions, with a higher relative abundance of rare species with extreme trait values. This pattern is consistent with the hypothesis that trait differences between rare and common species promote coexistence[13,14,36], for example, through limiting similarity[35] and associated density-dependent mechanisms[40] or facilitation[41]. For symmetrical distributions ($S^2 = 0$; Fig. 2), observed kurtoses were also lower than expected by chance. For the null assemblages, the y-intercept α at kurtosis ≈ 5 corresponds to a hyperbolic secant distribution (Fig. 2). In contrast, the observed y-intercept α at kurtosis ≈ 2 for SLA and kurtosis ≈ 3 for *H* correspond to uniform and normal distributions, respectively (Fig. 2). A uniform distribution implies strikingly high levels of trait diversity within dryland communities and the co-dominance of functionally contrasting species.

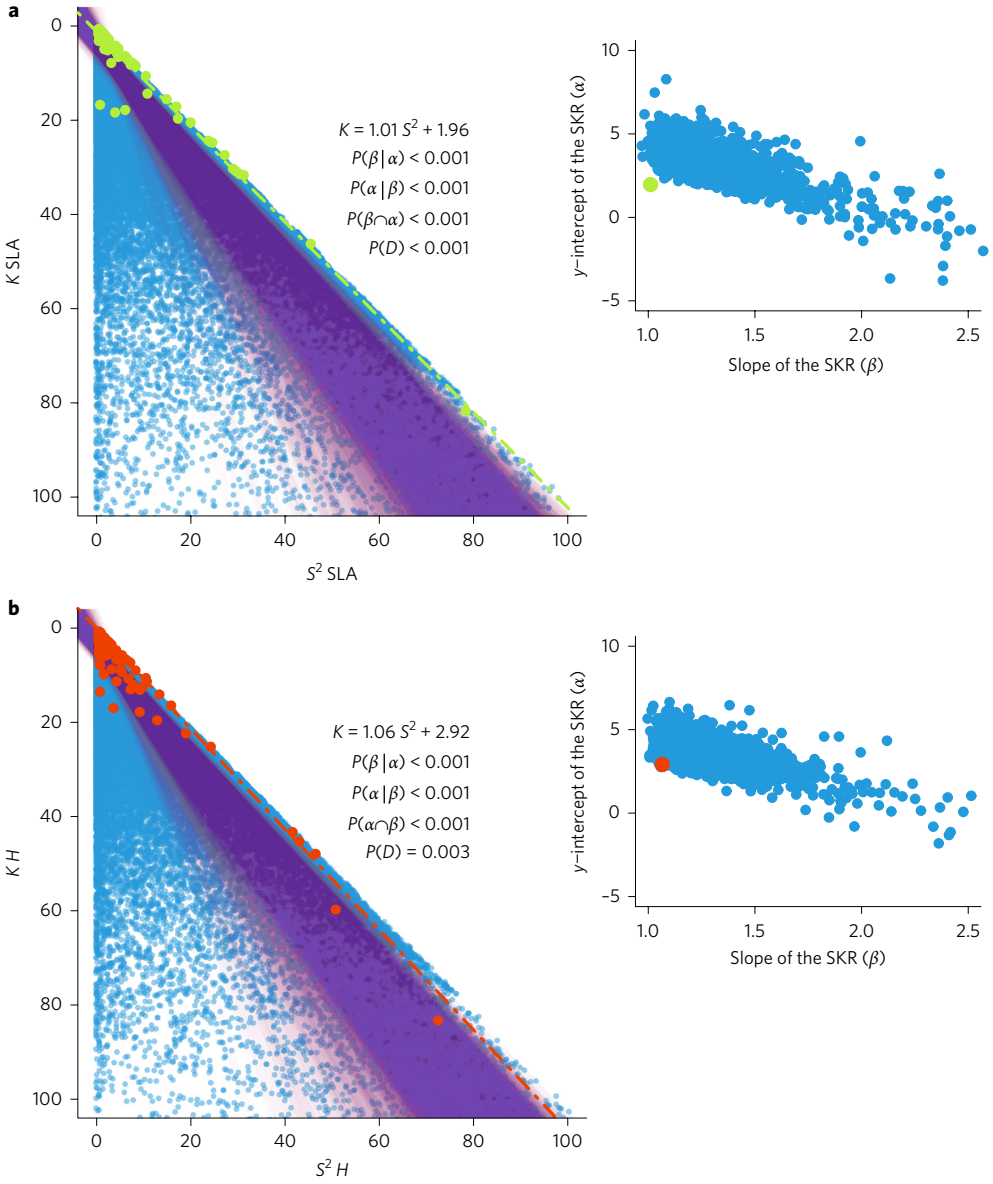

Figure 3 | Observed SKRs and deviation of from null expectations. a,**b**, Observed and null SKRs for SLA (**a**) and *H* (**b**). Blue dots represent the skewness and kurtosis values of random communities (2,000 randomizations × 124 communities); purple lines show the 2,000 random SKRs; green and red dots represent the observed 124 communities; the green and red dashed lines represent the observed SKRs for SLA and *H*, respectively. We indicate the equation for each observed SKR, and the conditional pseudo *P* values from null model 'richness' for the slope β, $P(\beta \mid \alpha)$, the *y*-intercept α, $P(\alpha \mid \beta)$, the whole model, $P(\beta \cap \alpha)$ and the distance to the lower boundary, $P(D)$ (see Table 1 and Supplementary Fig. 2 for details). Right panels indicate the relationship between the slopes β of the random SKRs and the random *y*-intercepts α (null parameters, blue dots); the green and red dots indicate the position of the observed parameters. The observed SKRs for SLA and *H* had significantly different *y*-intercepts (slope β: $F\text{-ratio}_{1,244} = 5308.16$, $P < 0.001$; *y*-intercept α: $F\text{-ratio}_{1,244} = 16.8$, $P < 0.0001$; Slope $\beta \times$ *y*-intercept α, $F\text{-ratio}_{1,244} = 3.68$, $P = 0.06$).

Trait distributions and ecosystem multifunctionality. The skewness and kurtosis of the trait–abundance distribution were the main biotic drivers of multifunctionality (Fig. 4). The model that included all abiotic and biotic predictors explained up to 66% (adjusted R^2) of the total variation observed in multifunctionality. Together, the skewness and kurtosis for SLA and *H* explained 38% of the variation in multifunctionality, which was greater than that explained by the mean and variance of these two traits (15%). Species richness explained only 5% of the variation in multifunctionality, which is comparable in magnitude to that reported in earlier studies[5] (see Supplementary Note 3 for more details).

To investigate the BEF relationship, ecologists have usually analysed the effect of biotic attributes such as species richness[1–3,5], community-weighted means of the trait–abundance distribution[8,11,15,25], or diversity indexes related to trait dispersion within communities (such as the variance of trait distribution)[10,17,23]. Our results do not contradict the findings of previous BEF studies, because we also found that species richness, the mean and variance of the trait distribution were all significant predictors of variation in multifunctionality. However, we showed that models including the skewness–kurtosis of the trait–abundance distributions had a much higher explanatory power for multifunctionality than models including only the mean and the variance of the trait–abundance distribution (see Supplementary Note 3). Considering the SKR represents a significant step forward in our ability to predict multifunctionality in global drylands (an additional ~38% explained variance compared with previous studies[5]).

Table 1 | Results from the null model for SLA and *H*.

				Direct assessments*						Distance to the lower boundary†		
Trait	Observed coefficient		R^2	Null model	$P(\beta)$	$P(\alpha)$	$P(\beta\|\alpha)$	$P(\alpha\|\beta)$	$P(\beta\cap\alpha)$	Trait	Null model	*P* value
SLA	β	1.236 ± 0.049	0.839	Frequency	0.279	0.313	0.002	0.002	0.001	SLA	Frequency	0.121
	α	2.149 ± 0.716		Richness	0.470	0.149	0.013	0.004	0.002		Richness	0.022
				Swap	0.766	0.118	0.047	0.007	0.006		Swap	0.119
log (SLA)	β	1.010 ± 0.019	0.956	Frequency	0.022	0.505	0.001	0.023	0.001	log (SLA)	Frequency	0.023
	α	1.961 ± 0.217		Richness	0.003	0.084	<0.001	<0.001	<0.001		Richness	<0.001
				Swap	0.371	0.196	0.031	0.016	0.006		Swap	0.011
H	β	1.482 ± 0.059	0.835	Frequency	0.711	0.504	0.455	0.322	0.229	*H*	Frequency	0.604
	α	2.52 ± 1.629		Richness	0.874	0.285	0.574	0.187	0.164		Richness	0.011
				Swap	0.830	0.379	0.562	0.257	0.213		Swap	0.663
log (H)	β	1.065 ± 0.020	0.955	Frequency	0.045	0.406	0.001	0.011	0.001	log (*H*)	Frequency	0.051
	α	2.921 ± 0.236		Richness	0.035	0.235	<0.001	<0.001	<0.001		Richness	0.004
				Swap	0.344	0.201	0.010	0.006	0.002		Swap	0.024

*Direct assessments of probabilities derived from the null models for the SKRs. The parameters β and α were tested separately, conditionally and jointly under the three randomization procedures. $P(\beta)$, probability of finding a lower random slope β during the randomization procedure than the observed slope β; $P(\alpha)$, probability of finding a lower random *y*-intercept α than the observed α; $P(\beta|\alpha)$, conditional probability of finding a lower random slope than the observed slope; $P(\alpha|\beta)$, conditional probability of finding a lower intercept in the randomizations than observed; $P(\beta\cap\alpha)$, probability of finding in the randomizations both a lower intercept and slope than observed. We indicate the regression parameters (estimate ± s.e.m., R^2) for observed SKRs. Pseudo *P* values below 0.05 indicate that the observed parameters are lower than the parameters expected by chance. †Distance to the lower boundary. We compared the distance of observed data and the predictions of the three null models for SLA and *H*. *P* values below 0.05 indicate that observed values are closer to the lower boundary of the SKR than expected by chance (see Methods for more information on each null model; Supplementary Note 2).

Linking a general assembly rule to ecosystem multifunctionality. We conducted a sensitivity analysis of the best-fitting model to explore how coordinated changes in the skewness and the kurtosis of the trait–abundance distributions affected multifunctionality (model 4, Fig. 4; see Supplementary Note 4 for more details on the sensitivity analysis). The two empirical SKRs predict a peak of multifunctionality to occur at their *y*-intercept α (skewness fixed at 0), that is, at the highest trait diversity predicted by the two empirical SKRs (green and red lines in Fig. 5). This peak is predicted to occur at the uniform distribution for SLA (SKR_{SLA} predicts a kurtosis value ≈ 2 at the *y*-intercept) and the normal distribution for *H* (SKR_H predicts a kurtosis value ≈ 3 at the *y*-intercept) described above (Fig. 2). Each empirical SKR also describes a ridge that minimizes the loss of multifunctionality for any change in the degree of skewness (see the green and red lines in Fig. 5). The existence of this ridge implies a tight coupling between the empirical SKRs and a maximization of multifunctionality in drylands.

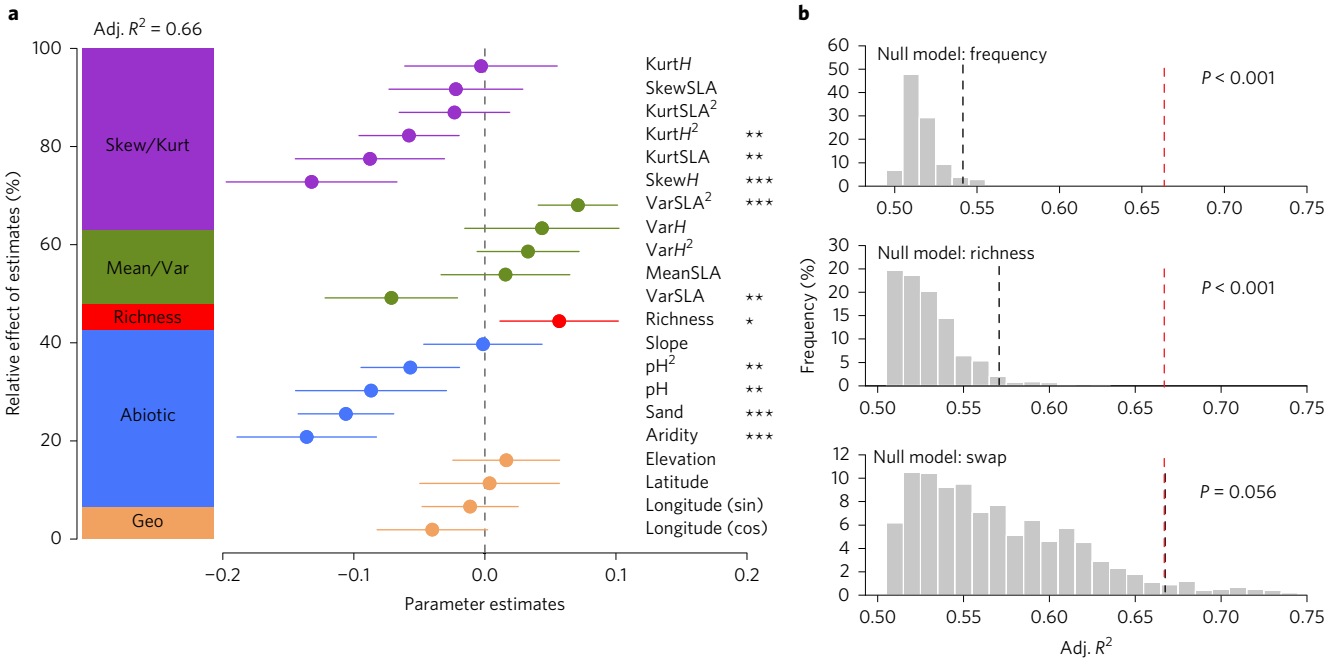

Figure 4 | Effect of abiotic and biotic factors on ecosystem multifunctionality. a, Average parameter estimates (standardized regression coefficients) of model predictors, associated 95% confidence intervals and relative importance of each factor, expressed as the percentage of explained variance. The adjusted (adj.) R^2 of the averaged model and the *P* value of each predictor are given as: $^*P < 0.05$; $^{**}P < 0.01$; $^{***}P < 0.001$. See Supplementary Table 3 for model selection. **b**, Frequency distribution of adj. R^2 from the null model analyses testing the relationship between trait–abundance distributions and multifunctionality. Black line is the 0.95 quantile of the null model prediction; red line is the observed adj. R^2. We provide pseudo *P* values for each null model (see Supplementary Note 3 for detailed results).

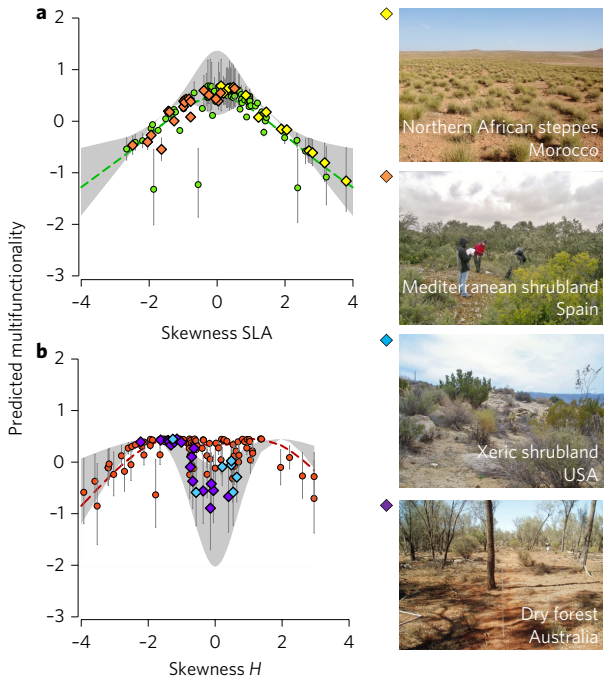

Figure 5 | Scaling relationship between the empirical SKRs and ecosystem multifunctionality. a,**b**, Predictions of the sensitivity analysis of the best selected multifunctionality model (model 4, Fig. 4; see Supplementary Note 4 for the detailed methods). Multifunctionality was predicted on a skewness axis for SLA (**a**) and *H* (**b**) for: (1) the two empirical SKRs where $K_{SLA} = 1.01\ S_{SLA}^2 + 1.96$ (green line in **a**) and $K_{Height} = 1.06\ S_{Height}^2 + 2.92$ (red line in **b**); (2) the lower boundary where $K_{Boundary} = S_{Boundary}^2 + 1$ (grey area: 95% confidence band); and (3) and the 124 communities studied (green and red dots). We located the position of emblematic dryland ecosystems from around the globe and dominated by contrasted flora (diamond symbols): **a** shows Northern African steppes dominates by *Stipa tenacissima* (yellow diamonds) and Mediterranean shrublands dominated by *Rosmarinus officinalis*, *Thymus vulgaris*, *Quercus coccifera* and *Q. ilex* (orange diamonds); **b** shows American xeric shrublands dominated by *Tetracoccus halli*, *Larrea tridentata* and *Ambroisia dumosa* (blue diamonds) and Australian woodlands dominated by *Casuarina cristata*, *Alectryon oleifolius* and *Eucalyptus* sp. (purple diamonds). Within each ecosystem, changes in the shape of the trait abundance distributions can be used to monitor changes in multifunctionality. Photos D. Eldridge, N.G. and F.T.M.

Using the same randomization test applied across communities (see Methods; Supplementary Note 5), we found that the relationship between trait–abundance distributions observed within communities and multifunctionality also cannot be explained by chance (Fig. 4b). The two empirical SKRs corresponded to the unique sets of trait distributions able to explain multifunctionality with such a high predictive power (Fig. 4b). Results were robust to the three randomization scenarios employed, including the most highly constrained null model based on the local species composition and trait pool observed within communities (Supplementary Note 3). Our analysis thus supports the existence of a unique scaling relationship linking plant functional traits (SLA and *H*), the distribution of their abundance within communities and multiple ecosystem functions.

It is noteworthy that increasing trait diversity to its highest potential values defined by the lower boundary of the constraint triangle does not necessarily increase multifunctionality (Fig. 5b). For example, decreasing the kurtosis value for *H* beyond the normal distribution towards a kurtosis value of 1 (that is, the lower boundary) had a strong detrimental effect on the multifunctionality of xeric shrublands and dry forests (blue and purple diamonds in Fig. 5b, respectively; see also Supplementary Note 4). We observed (1) a maximized multifunctionality state closer to a normal distribution (*y*-intercept $\alpha \approx 3$, along red line in Fig. 5b); and (2) a reduced multifunctionality state closer to the lower boundary (see the shaded area in Fig. 5b). The two empirical SKRs not only show that high trait diversity is needed to sustain multifunctionality, but also precisely quantify how much diversity is required to maximize it locally.

Our study suggests that SLA and *H*—two key plant attributes[26]—can be used as efficient functional markers (*sensu* ref. [15]) to scale-up trait diversity to the ecosystem level. However, the mechanistic linkages between these two traits and multifunctionality remain to be explored. In this context, other proximal traits known to impact ecosystem functioning should be considered in future studies, such as below-ground traits[42] (such as rooting depth), element stoichiometry[43] (such as C:N ratio) and litter traits[44] (such as lignin content). Also, intraspecific trait variability has been shown to modulate community assembly[45,46] and ecosystem functioning[47], and was not included in our study. How intraspecific trait variability modulates multifunctionality on a local and global scale remains largely unexplored. Lastly, our study focuses only on perennial plants. The role of functional diversity of annual plants, which can account for a large proportion of plant species diversity in drylands, certainly deserves additional attention.

Conclusion

We uncovered a general family of trait–abundance distributions operating on the biome scale that quantify the maxima of trait diversity needed to sustain multifunctionality in global drylands (Fig. 5). Biome-scale distributions emerged from local scale processes of maximization operating within communities, and highlight a tight coupling between community assembly and ecosystem functioning in global drylands. By quantifying a scaling relationship between the abundance distribution of functional traits and maximized multifunctionality, our analysis suggests that trait distributions could be used to assess the functional consequences of biodiversity loss in terrestrial ecosystems, and to guide management efforts aimed at maintaining key ecosystem services linked to productivity and soil fertility.

Methods

Characteristics of the study sites. We obtained field data from 124 sites located in 13 countries (Argentina, Australia, Chile, China, Ecuador, Israel, Kenya, Mexico, Morocco, Spain, Tunisia, USA and Venezuela; Fig. 1). These sites are a subset of the global network of sites from ref. [5]. Our data set includes representative sites from the main vegetation types found in drylands, which differ widely in plant species richness (5 to 44 species per site, average = 16.44) and environmental conditions[32] (mean annual temperature and precipitation ranged from −1.8 to 27.8 °C and from 79 to 1,177 mm, respectively).

Trait–abundance distributions. We focused on two key plant functional traits[26]: SLA, which indexes leaf-level carbon gain strategies[48]; and *H*, which reflects a trade-off for biophysical constraints in determining water fluxes within the plant[49], and is related to competitive ability[33]. We quantified the abundance distributions of these traits, which describe the relative abundance of each trait value within each of the 124 communities, by using two independent data sets: (1) a detailed data set containing the percent cover of each perennial plant species measured in 80 quadrats of 2.25 m^2 within each site, where the sum of the cover for each species is used as a proxy of species abundance at each site[5]; and (2) data for mean trait value per species for SLA and *H* retrieved from the TRY database[24]. The number of sites selected was based on the availability of trait data. We selected those sites for which trait data were available for all the most common perennial plant species that together accounted for a cumulative relative abundance >80%[50] (averaged cumulative relative abundance for SLA = 94.3 ± 6.5 s.e.m.; for *H* = 96.6 ± 5.24 s.e.m.). Therefore, our approach focused on the dominant and subordinate species, known to impact the most ecosystem functioning, according to the mass ratio hypothesis[51]. We acknowledge that our analyses do not account for the effect of species with very low abundance. In total, trait data were available for 316 and 526 plant species out of 622 species for SLA and *H*, respectively.

We calculated the mean, variance, skewness and kurtosis of the 124 trait–abundance distributions[25,32] for SLA and *H* separately as follows:

$$\text{Mean}_j = \sum_i^n p_i T_i \quad (4)$$

$$\text{Variance}_j = \sum_i^n p_i (T_i - \text{Mean}_j)^2 \quad (5)$$

$$\text{Skewness}_j = \sum_i^n \frac{p_i (T_i - \text{Mean}_j)^3}{\text{Variance}_j^{3/2}} \quad (6)$$

$$\text{Kurtosis}_j = \sum_i^n \frac{p_i (T_i - \text{Mean}_j)^4}{\text{Variance}_j^{2}} \quad (7)$$

where p_i and T_i are the relative abundance and the trait value of the species i in the community j, respectively, and n is the total number of species in a community with available trait values. For each community, the sum of relative abundance is equal to 100%, that is, $\Sigma = 1$. In contrast to the mean and the variance, the skewness and the kurtosis are unitless. The weighted abundance trait distribution quantifies how much relative abundance exhibits each trait value present in a given community, and provides the shape of the distribution (see Supplementary Note 1).

Assessing multifunctionality. We estimated multifunctionality for the 124 selected sites using plant productivity, soil enzymatic activities (that is, activity of phosphatase and β-glucosidase), ammonification and potential N transformation rate. These variables (hereafter functions) were uncorrelated among themselves (Supplementary Table 1) and measure either 'true' ecosystem functions (*sensu* ref. [52]; for example, potential N transformation rate, productivity) or are key properties/processes (*sensu* ref. [53]; for example, soil enzymatic activities), which together constitute a good proxy for nutrient cycling, biological productivity and build-up of nutrient pools. The ecosystem functions evaluated are also considered to be critical determinants of ecosystem functioning in drylands[5,28,43,54,55]. We used a conservative approach to quantifying multifunctionality by minimizing the number of ecosystem functions considered. However, including additional ecosystem functions related to carbon, nitrogen and phosphorus stocks and cycling when assessing multifunctionality did not affect our results (see Supplementary Note 3).

Plant productivity was quantified using the normalized difference vegetation index (NDVI) at the site level, which acts as a proxy of photosynthetic activity of terrestrial ecosystems for a given composite period[28,56]. These data were obtained with a resolution of 250 m from the moderate resolution imaging spectroradiometer aboard NASA's Terra satellites (http://daac.ornl.gov/index.shtml). Here, we used NDVI values obtained for the months before, during and after sampling at each of the surveyed plots averaged across a period of 13 yr (2000 to 2013). Soil variables were measured from soil samples (0 and 7.5 cm depth) collected under the canopy of the dominant perennial plants, and in open areas devoid of vascular vegetation as described in refs [5,43]. The different ecosystem functions measured were used to obtain a multifunctionality index (*M*), as described in ref. [5]. First, we standardized separately the five ecosystem functions (*F*) using the *Z*-score transformation:

$$Z - \text{Score}_{ij} = \frac{F_{ij} - \text{Mean } F_i}{\text{s.d. } F_i} \quad (8)$$

where F_{ij} is the value of an ecosystem function i in the community j, and mean and s.d. F_i are the mean and the standard deviation of the ecosystem function F_i calculated for the 124 studied communities, respectively.

We then obtained *M* for each community j as the average of the *Z*-scores of the five ecosystem functions i assessed.

M has good statistical properties[5,21] and is a straightforward and easily interpretable measure of multifunctionality[21]. All selected single functions were positively correlated with *M* (Supplementary Table 1a).

Environmental and spatial variables measured. We summarized the climatic features of the studied sites using aridity, a major determinant of ecosystem structure and functioning in drylands worldwide[54,55]. We obtained values of the aridity index (AI; precipitation/potential evapotranspiration) from ref. [57], which uses the data interpolations provided by Worldclim[58]. To facilitate the interpretation of results, we calculated the aridity level for each site as 1 − AI, so higher values of this aridity level indicate drier conditions[43]. Aridity is strongly correlated with annual mean precipitation in our data set ($r = -0.84$).

We summarized local topo-edaphic parameters at each site using slope angle (as a surrogate of topography), soil sand content and soil pH. These variables, measured as described in ref. [5], play key roles in the availability of water and nutrients in drylands[57], and are major drivers of the composition and diversity of plant and microbial communities[28,32]. Clay and silt content were not used in our analyses due to their correlation with sand content ($r = -0.52$ and -0.55, respectively). We also considered the elevation, latitude and longitude of the study sites in our analyses to account for potential effects of spatial autocorrelation among them[5,32]. We used the sinus and cosinus of the longitude to avoid any bias due to intrinsic circularity of longitude in the models.

Community-level analyses. The mathematical relationship between the skewness (*S*) and kurtosis (*K*) of the trait–abundance distributions (SKR) takes the form of an inequality[37] (1), where $K = S^2 + 1$ defines the lower boundary to the SKR (Fig. 2; see Supplementary Note 1 for a full mathematical demonstration of the SKR, and for more information on its implications and use in various scientific fields).

We used a null model approach to test whether observed SKRs differ from random expectations. Using the package PICANTE[59] in the R statistical software, version 3.1.1[60], we constructed three null models with increasing constraints on the randomization procedure. We performed 2,000 randomizations for each null model. We assumed in the first null model that local communities reflect random distributions of species drawn from the global species pool. In this null model, species abundance was shuffled across communities using the function 'frequency' in PICANTE. This procedure kept the abundance of each species constant on the global scale, but allowed the distributions of species richness and abundance to randomly vary within communities. We assumed in the second null model that these distributions were fixed within communities (function 'richness' in PICANTE). This null model randomized the trait values across species to break out the observed relationship between species traits and abundance. The randomization of trait values avoided any bias in null predictions promoted by local variations in the number and cover of species observed on the community scale[61]. In the third null model, we restricted species richness and the range of trait values to those already filtered by the environment within communities (function 'independentswap' in PICANTE). Therefore, trait values are randomly shuffled across the species occurring in each community.

We calculated the mean, variance, skewness and kurtosis of the trait–abundance distributions for SLA and *H* for each of the 2,000 randomizations, and for each of the null models used. These were calculated using both raw and log-transformed trait values, as log-transformation may impact the level of detection of non-random processes[62]. We calculated the 2,000 random relationships between skewness and kurtosis ($\text{SKR}_{\text{random}}$; equation (1)). Then we extracted both the slope (β_{random}) and the *y*-intercept (α_{random}) of the 2,000 $\text{SKR}_{\text{random}}$. We then compared β_{random} and α_{random} with observed parameters of the SKR (β_{obs} and α_{obs}) for each of the three independent null models used. We used two different approaches to assess whether the observed SKR significantly differed from $\text{SKR}_{\text{random}}$.

Direct assessment. We compared observed parameters of the SKR (that is, the slope β and *y*-intercept α) with those generated by the three null models. Importantly, null models predicted a negative relationship between β_{random} and α_{random}, indicating a dependency between random parameters (Supplementary Fig. 1). Therefore, we used the Bayes theorem to calculate conditional probabilities for β and α (Supplementary Fig. 1). Specifically, we calculated:

- An initial pseudo *P* value for β ($P(\beta)$), generated by comparing β_{obs} with the probability distribution of β_{random} (Supplementary Fig. 1a). We counted the frequency with which we generated a random slope (β_{random}) smaller than the observed slope (β_{obs}). We then calculated $P(\beta)$ as the number of randomizations with $\beta_{\text{random}} \leq \beta_{\text{obs}}$ divided by the total number of randomizations. An observed slope β_{obs} significantly lower than the probability distribution of β_{random} indicates that the slope of the observed SKR is less steep than expected by chance. Any change in the skewness of the distributions leads to a slower increase in kurtosis than expected by chance.
- A second pseudo *P* value for α ($P(\alpha)$; Supplementary Fig. 1b). To do so, we counted the frequency of observing a *y*-intercept expected by chance (α_{random}) being lower than the observed *y*-intercept (α_{obs}). We then calculated $P(\alpha)$ as the number of randomizations with $\alpha_{\text{random}} \leq \alpha_{\text{obs}}$ divided by the total number of randomizations. An observed *y*-intercept (α_{obs}) significantly lower than expected by chance indicates a lower kurtosis at the *y*-intercept than expected by chance.
- A third pseudo *P* value for α taking into account the observed slope β (α if β: conditional *P* value = $P(\alpha|\beta)$; Supplementary Fig. 1c). We obtained $P(\alpha|\beta)$ by counting the number of observations with an *y*-intercept expected by chance (α_{random}) lower than the observed *y*-intercept (α_{obs}) within the subset of randomizations in which β_{obs} is lower than the slope expected by chance (β_{random}).
- A fourth pseudo *P* value for β taking into account the observed *y*-intercept α (β if α: conditional *P* value = $P(\beta|\alpha)$; Supplementary Fig. 1d). We calculated $P(\beta|\alpha)$ by using the Bayes theorem:

$$P(\beta|\alpha) = P(\beta) \times P(\alpha|\beta) / P(\alpha) \quad (9)$$

- A fifth pseudo *P* value including β and α together ($\beta + \alpha$, $P(\beta \cap \alpha)$; Supplementary Fig. 1e). We followed the Bayes equation to calculate $P(\beta \cap \alpha)$:

$$P(\beta \bigcap \alpha) = P(\beta) \times P(\alpha|\beta) \quad (10)$$

$P(\beta \cap \alpha)$ represents the probability to observe a whole model with both a slope and a y-intercept (β_{obs} and α_{obs}) being lower than expected by chance.

Distance to the lower boundary: we used a complementary approach to assess whether the observed SKR differs from SKR_{random} by testing whether observed kurtoses of each of the 124 communities sampled were significantly closer to the lower boundary than the random data. The lower boundary defines the lowest level of kurtosis that can be expected for any degree of skewness (Fig. 2). If the 124 observed communities are closer on average to the lower boundary than expected by chance, we can conclude that trait diversity within communities is maximized for any degree of skewness. In each randomization event, we calculated the distances to the kurtosis at the lower boundary (K_{bound}) for both random and observed kurtosis values for each community j, where K_{bound} is defined as:

$$K_{boundj} = S_j^2 + 1 \quad (11)$$

where S^2_j is the skewness square value of the community j. We then calculated the distance (D) of the community j to the lower boundary as:

$$D_j = K_j - K_{bound} \quad (12)$$

We fitted an ANOVA model using the function 'aov()' in R to compare the observed distances to the lower boundary and those obtained for each randomization. A positive estimate of the ANOVA comparison indicates that the observed kurtosis was closer to the lower boundary than expected by chance. We performed 2,000 randomizations for each of the three null models and stored all resulting estimates from the ANOVA. Using these data, we calculated a pseudo P value based on the frequency of observing a slope ≤ 0 within the distribution of 2,000 slopes.

Ecosystem-level analyses. We used multiple regression models to assess the effect of trait–abundance distribution on multifunctionality. We built four competing models including as predictors: (1) spatial (latitude, cos-longitude, sin-longitude and elevation) and abiotic (aridity, soil sand content, slope angle and pH considering a quadratic term for pH only) variables ('abiotic' model); (2) all variables of the model 'abiotic' plus the mean and the variance of trait–abundance distributions for SLA and H ('biotic low moments' model); (3) all variables of the model 'abiotic' plus the skewness and the kurtosis of trait–abundance distributions for SLA and H ('biotic high moments' model); and (4) all variables of the model 'abiotic' plus the mean, variance, skewness and kurtosis of trait–abundance distributions for SLA and H ('biotic all moments' model). In the four models we also included species richness as predictor to control for its potential effects on multifunctionality[5]. Species richness was not correlated with the four moments of the trait–abundance distributions for both H and SLA (Supplementary Table 2), except in the case of the variance, where a positive trend was observed ($r < 0.40$ for H and SLA). We also considered quadratic terms for the mean, variance and kurtosis both for H and SLA to assess potential non-linear effects of these variables on multifunctionality[23]. Note that we never included a quadratic term for skewness because $K = \beta S^2 + \alpha$, equation (1). In the final models we did not include quadratic terms for the abiotic variables (that is, aridity, sand) with the exception of soil pH, for the sake of simplicity.

We used a model selection procedure based on corrected Akaike's information criterion (AICc; $\Delta AICc < 2$)[63] to select the best predictors of multifunctionality. This procedure was performed using the function 'dredge' in the R package MuMIn[64]. Model averaging was performed based on AICc weights when multiple models were selected. Model residuals were inspected for constant variance and normality. All predictors and response variables were standardized before analyses using the Z-score to interpret parameter estimates on a comparable scale. Predictors were log-transformed when necessary before analysis to meet the assumptions of the tests used.

We evaluated the relative importance of the predictors under consideration as drivers of multifunctionality. To do so, we calculated the relative effect of the parameter estimates for each of the predictors compared with the effect of all parameter estimates in the model. This method is similar to a variance decomposition analysis because we transformed all predictors to Z-scores before analysis. The following five identifiable variance fractions were examined: (1) spatial variables; (2) abiotic variables; (3) species richness; (4) mean and variance; and (5) skewness and kurtosis of trait–abundance distributions.

We evaluated how the observed SKRs explained variations in multifunctionality using the final best-fitting models. Whenever kurtosis and kurtosis squared for SLA and H were selected in the averaged model, we used their averaged parameter estimates to model its effects on multifunctionality. All other predictors selected in the averaged model were treated as constant and fixed to their mean (that is, 0, as all predictors were transformed to Z-scores; see Supplementary Note 4 for more details). Finally, we used the same null model approach developed at the community level to test whether the relationship between trait–abundance distributions and multifunctionality could be observed by chance (see Supplementary Note 5 for more details).

Data availability. All the data used in the primary analyses and associated R codes are available from figshare: https://figshare.com/s/053837c4fa852f035448.

Received 17 October 2016; accepted 8 March 2017; published 18 April 2017

References

1. Schmid, B. *et al.* in *Biodiversity, Ecosystem Functioning, and Human Wellbeing: An Ecological and Economic Perspective* (eds Naeem, S., Bunker, D. E., Hector, A., Loreau, M. & Perrings, C.) 14–29 (Oxford Univ. Press, 2009).
2. Hooper, D. U. *et al.* Effects of biodiversity on ecosystem functioning: a consensus of current knowledge. *Ecol. Monogr.* **75,** 3–35 (2005).
3. Cardinale, B. J. *et al.* Biodiversity loss and its impact on humanity. *Nature* **486,** 59–67 (2012).
4. Gamfeldt, L., Hillebrand, H. & Jonsson, P. R. Multiple functions increase the importance of biodiversity for overall ecosystem functioning. *Ecology* **89,** 1223–1231 (2008).
5. Maestre, F. T. *et al.* Plant species richness and ecosystem multifunctionality in global drylands. *Science* **335,** 214–218 (2012).
6. Grace, J. B. *et al.* Integrative modelling reveals mechanisms linking productivity and plant species richness. *Nature* **529,** 390–393 (2016).
7. Gamfeldt, L. *et al.* Marine biodiversity and ecosystem functioning: what's known and what's next? *Oikos* **124,** 252–265 (2015).
8. Lavorel, S. & Garnier, E. Predicting changes in community composition and ecosystem functioning from plant traits: revisiting the Holy Grail. *Funct. Ecol.* **16,** 545–556 (2002).
9. Naeem, S. & Wright, J. P. Disentangling biodiversity effects on ecosystem functioning: deriving solutions to a seemingly insurmountable problem. *Ecol. Lett.* **6,** 567–579 (2003).
10. Díaz, S. *et al.* Incorporating plant functional diversity effects in ecosystem service assessments. *Proc. Natl Acad. Sci. USA* **104,** 20684–20689 (2007).
11. Violle, C. *et al.* Let the concept of trait be functional! *Oikos* **116,** 882–892 (2007).
12. McGill, B. J., Enquist, B. J., Weiher, E. & Westoby, M. Rebuilding community ecology from functional traits. *Trends Ecol. Evol.* **21,** 178–185 (2006).
13. Mayfield, M. M. & Levine, J. M. Opposing effects of competitive exclusion on the phylogenetic structure of communities. *Ecol. Lett.* **13,** 1085–1093 (2010).
14. Maire, V. *et al.* Habitat filtering and niche differentiation jointly explain species relative abundance within grassland communities along fertility and disturbance gradients. *New Phytol.* **196,** 497–509 (2012).
15. Garnier, E. *et al.* Plant functional markers capture ecosystem properties during secondary succession. *Ecology* **85,** 2630–2637 (2004).
16. Naeem, S. *et al.* Declining biodiversity can alter the performance of ecosystems. *Nature* **368,** 734–737 (1994).
17. de Bello, F. *et al.* Towards an assessment of multiple ecosystem processes and services via functional traits. *Biodivers. Conserv.* **19,** 2873–2893 (2010).
18. Gross, N., Suding, K. N., Lavorel, S. & Roumet, C. Complementarity as a mechanism of coexistence between functional groups of grasses. *J. Ecol.* **95,** 1296–1305 (2007).
19. Mouillot, D., Villéger, S., Scherer-Lorenzen, M. & Mason, N. W. Functional structure of biological communities predicts ecosystem multifunctionality. *PLoS ONE* **6,** e17476 (2011).
20. Funk, J. L. *et al.* Revisiting the Holy Grail: using plant functional traits to understand ecological processes. *Biol. Rev.* http://dx.doi.org/10.1111/brv.12275 (2016).
21. Byrnes, J. E. *et al.* Investigating the relationship between biodiversity and ecosystem multifunctionality: challenges and solutions. *Methods Ecol. Evol.* **5,** 111–124 (2014).
22. Lefcheck, J. S. *et al.* Biodiversity enhances ecosystem multifunctionality across trophic levels and habitats. *Nat. Commun.* **6,** 6936 (2015).
23. Valencia, E. *et al.* Functional diversity enhances the resistance of ecosystem multifunctionality to aridity in Mediterranean drylands. *New Phytol.* **206,** 660–671 (2015).
24. Kattge, J. *et al.* TRY–a global database of plant traits. *Glob. Change Biol.* **17,** 2905–2935 (2011).
25. Enquist, B. J. *et al.* Scaling from traits to ecosystems: developing a general trait driver theory via integrating trait-based and metabolic scaling theories. *Adv. Ecol. Res.* **52,** 249–318 (2015).
26. Díaz, S. *et al.* The global spectrum of plant form and function. *Nature* **529,** 167–171 (2016).
27. Grime, J. P. *Plant Strategies, Vegetation Processes, and Ecosystem Properties.* (John Wiley & Sons, 2006).
28. Delgado-Baquerizo, M. *et al.* Microbial diversity drives multifunctionality in terrestrial ecosystems. *Nat. Commun.* **7,** 10541 (2016).
29. Cristelli, M. *Complexity in Financial Markets* 141–150 (Springer, 2014).
30. Cornwell, W. K. & Ackerly, D. D. Community assembly and shifts in plant trait distributions across an environmental gradient in coastal California. *Ecol. Monogr.* **79,** 109–126 (2009).
31. Kraft, N. J., Valencia, R. & Ackerly, D. D. Functional traits and niche-based tree community assembly in an Amazonian forest. *Science* **322,** 580–582 (2008).

32. Le Bagousse-Pinguet, Y. *et al.* Testing the environmental filtering concept in global drylands. *J. Ecol.* http://dx.doi.org/10.1111/1365-2745.12735 (2017).
33. Schamp, B. S., Chau, J. & Aarssen, L. W. Dispersion of traits related to competitive ability in an old-field plant community. *J. Ecol.* **96,** 204–212 (2008).
34. Gross, N. *et al.* Linking individual response to biotic interactions with community structure: a trait-based framework. *Funct. Ecol.* **23,** 1167–1178 (2009).
35. MacArthur, R. & Levins, R. The limiting similarity, convergence, and divergence of coexisting species. *Am. Nat.* **101,** 377–385 (1967).
36. Chesson, P. General theory of competitive coexistence in spatially-varying environments. *Theor. Popul. Biol.* **58,** 211–237 (2000).
37. Cullen, A. C. & Frey, H. C. *Probabilistic Techniques in Exposure Assessment: A Handbook for Dealing with Variability and Uncertainty in Models and Inputs* (Springer, 1999).
38. Keddy, P. A. Assembly and response rules: two goals for predictive community ecology. *J. Veg. Sci.* **3,** 157–164 (1992).
39. Weiher, E. *et al.* Advances, challenges and a developing synthesis of ecological community assembly theory. *Phil. Trans. R. Soc. B* **366,** 2403–2413 (2011).
40. Levine, J. M. & HilleRisLambers, J. The importance of niches for the maintenance of species diversity. *Nature* **461,** 254–257 (2009).
41. Gross, N., Liancourt, P., Butters, R., Duncan, R. P. & Hulme, P. E. Functional equivalence, competitive hierarchy and facilitation determine species coexistence in highly invaded grasslands. *New Phytol.* **206,** 175–186 (2015).
42. Bardgett, R. D., Mommer, L. & De Vries, F. T. Going underground: root traits as drivers of ecosystem processes. *Trends Ecol. Evol.* **29,** 692–699 (2014).
43. Delgado-Baquerizo, M. *et al.* Decoupling of soil nutrient cycles as a function of aridity in global drylands. *Nature* **502,** 672–676 (2013).
44. García-Palacios, P., McKie, B. G., Handa, I. T., Frainer, A & Hättenschwiler, S. The importance of litter traits and decomposers for litter decomposition: a comparison of aquatic and terrestrial ecosystems within and across biomes. *Funct. Ecol.* **30,** 819–829 (2016).
45. Bolnick, D. I. *et al.* Why intraspecific trait variation matters in community ecology. *Trends Ecol. Evol.* **26,** 183–192 (2011).
46. Siefert, A. *et al.* A global meta-analysis of the relative extent of intraspecific trait variation in plant communities. *Ecol. Lett.* **18,** 1406–1419 (2015).
47. Crutsinger, G. M. *et al.* Plant genotypic diversity predicts community structure and governs an ecosystem process. *Science* **313,** 966–968 (2006).
48. Wright, I. J. *et al.* The worldwide leaf economics spectrum. *Nature* **428,** 821–827 (2004).
49. Enquist, B. J. Universal scaling in tree and vascular plant allometry: toward a general quantitative theory linking plant form and function from cells to ecosystems. *Tree Physiol.* **22,** 1045–1064 (2002).
50. Pakeman, R. J. & Quested, H. M. Sampling plant functional traits: what proportion of the species need to be measured? *Appl. Veg. Sci.* **10,** 91–96 (2007).
51. Grime, J. P. Benefits of plant diversity to ecosystems: immediate, filter and founder effects. *J. Ecol.* **86,** 902–910 (1998).
52. Reiss, J., Bridle, J. R., Montoya, J. M. & Woodward, G. Emerging horizons in biodiversity and ecosystem functioning research. *Trends Ecol. Evol.* **24,** 505–514 (2009).
53. Jax, K. *Ecosystem Functioning* (Cambridge Univ. Press, 2010).
54. Whitford, W. G. *Ecology of Desert Systems* (Academic, 2002).
55. Reynolds, J. F. *et al.* Global desertification: building a science for dryland development. *Science* **316,** 847–851 (2007).
56. Pettorelli, N. *et al.* Using the satellite-derived NDVI to assess ecological responses to environmental change. *Trends Ecol. Evol.* **20,** 503–510 (2005).
57. Loik, M. E., Breshears, D. D., Lauenroth, W. K. & Belnap, J. A multi-scale perspective of water pulses in dryland ecosystems: climatology and ecohydrology of the western USA. *Oecologia* **141,** 269–281 (2004).
58. Hijmans, R. J., Cameron, S. E., Parra, J. L., Jones, P. G. & Jarvis, A. Very high resolution interpolated climate surfaces for global land areas. *Int. J. Climatol.* **25,** 1965–1978 (2005).
59. Kembel, S. W. *et al.* Picante: R tools for integrating phylogenies and ecology. *Bioinformatics* **26,** 1463–1464 (2010).
60. R Core Team. R: A Language and Environment for Statistical Computing (R Foundation for Statistical Computing, 2014).
61. Gotelli, N. J. & Entsminger, G. L. Swap and fill algorithms in null model analysis: rethinking the knight's tour. *Oecologia* **129,** 281–291 (2001).
62. Májeková, M. *et al.* Evaluating functional diversity: missing trait data and the importance of species abundance structure and data transformation. *PLoS ONE* **11,** e0149270 (2016).
63. Burnham, K. P. & Anderson, D. R. *Model Selection and Multimodel Inference: A Practical Information-Theoretic Approach* (Springer, 2002).
64. Bartoń, K. MuMIn: multi-model inference. R package v. 1 (R Foundation for Statistical Computing, 2013).

Acknowledgements

This work was funded by the European Research Council (ERC) under the European Community's Seventh Framework Programme (FP7/2007-2013)/ERC grant agreement 242658 (BIOCOM). Y.L.B.P was supported by a Marie Sklodowska-Curie Actions Individual Fellowship within the European programme Horizon 2020 (DRYFUN project 656035). N.G. was support by the AgreenSkills+ fellowship programme, which has received funding from the EU's Seventh Framework Programme under grant agreement FP7-609398 (AgreenSkills+ contract). F.T.M. acknowledges support from the ERC (grant agreement 647038; BIODESERT). N.J.G. was supported by the US NSF DEB 1257625, NSF DEB 1144055 and NSF DEB 1136644. M.B. was supported by an FPU fellowship from the Spanish Ministry of Education, Culture and Sports (ref. AP2010-0759). We are very grateful to L. Börger, D. Eldridge, M. García-Gómez, V. Maire, M. Robson, H. Saiz and C. Violle for providing comments on previous versions of the manuscript, and to C. Mañá for explaining the statistical background on the skewness–kurtosis relationship.

Author contributions

N.G., Y.L.B.P. and P.L. developed the original idea. F.T.M. designed and collected the 'drylands' data set. N.G., Y.L.B.P., N.J.G. and M.B. conducted the statistical analyses. N.G., Y.L.B.P. and P.L. wrote the article, with major contributions from F.T.M., M.B. and N.J.G.

Additional information

Supplementary information is available for this paper.

Reprints and permissions information is available at www.nature.com/reprints.

Correspondence and requests for materials should be addressed to N.G., Y.L.B.-P. and P.L.

How to cite this article: Gross, N. *et al.* Functional trait diversity maximizes ecosystem multifunctionality. *Nat. Ecol. Evol.* **1,** 0132 (2017).

Competing interests

The authors declare no competing financial interests.